14th International Symposium on Turbulence and Shear Flow Phenomena (TSFP14)
Heidelberg, Germany, July 28–31, 2026

EXPERIMENTAL ANALYSIS OF TRANSONIC BUFFET ON A SWEPT WING AT HIGH REYNOLDS NUMBER

Tobias Huber
Department 03 - Mechanical, Automotive and Aeronautical Engineering
Hochschule München University of Applied Sciences
Dachauer Straße 98b, 80335 München, Germany
tobias.huber@hm.edu

Christopher J. Schauerte
Institute of Aerodynamics and Chair of Fluid Mechanics
RWTH Aachen University
Wüllnerstraße 5a, 52062 Aachen, Germany
c.schauerte@aia.rwth-aachen.de

Johannes Bosbach, Robert Konrath, Reinhard Geisler, and Florian Philipp
Institute of Aerodynamics and Flow Technology
German Aerospace Center
Bunsenstraße 10, 37073 Göttingen, Germany
Johannes.Bosbach@dlr.de

Anne-Marie Schreyer
Department 03 - Mechanical, Automotive and Aeronautical Engineering
Hochschule München University of Applied Sciences
Dachauer Straße 98b, 80335 München, Germany
anne-marie.schreyer@hm.edu

ABSTRACT

The flow phenomenon of transonic buffet severely limits the flight envelope of modern passenger aircraft. To contribute to providing the required understanding to eventually expand these limits while maintaining the highest safety standards, we analyzed the velocity field around and in the wake of the wing of a full-span, generic passenger aircraft model under buffet conditions in detail. Our study provides rare insights into the buffet phenomenon at a high, flight realistic Reynolds number of $Re = 12.9 \cdot 10^6$. The data was measured in the European Transonic Windtunnel (ETW) by means of the cryogenic Particle Image Velocimetry (cryoPIV) technique.

INTRODUCTION

The commercially relevant transonic flight regime poses a major challenge to modern aircraft design as it is prone to the occurrence of the unsteady flow phenomenon of transonic buffet. On the wings of commercial aircraft, at cruise conditions, a large region of supersonic flow forms in the front part of the wing. This region is terminated by a normal shock wave (Stanewsky & Basler (1990)). While the occurrence of such mostly steady compressibility effects is inevitable at the conditions prevailing at the edge of the flight envelope, under certain combinations of upstream Mach number, angle of attack, and Reynolds number, the highly unsteady flow mode of transonic buffet can occur.

Shock buffet is, inter alia, associated with a highly unsteady flow field (Molton *et al.* (2013)), severe oscillations of the lift coefficient (Crouch *et al.* (2009)), and fluctuating aerodynamic forces on the aircraft (Benoit & Legrain (1987)). While the lift fluctuations are unfavorable by themselves, their mechanical coupling with the airframe can lead to a detrimental structural response, referred to as buffeting. Therefore, transonic buffet not only entails drag penalties and diminishes the aerodynamic performance, it may even result in serious damage to the wing structure (Eckstrom *et al.*, 1990; Nicholas *et al.*, 2017). As certification requirements specify a safety margin of 30% to the onset of buffet for commercial aircraft (Kenway & Martins (2017)), the phenomenon constrains the usable range of the flight envelope (Molton *et al.* (2013)).

For 2D wings or airfoils, buffet manifests itself in a quasi-sinusoidal shock motion at a distinct frequency. On 3D swept wings of modern aircraft, significant spanwise dynamics occur, which are characterized by a superposition of a back-and-forth motion of the shock and a spanwise propagation of cellular shock distortion patterns (Iovnovich & Raveh (2015)). These phenomena add a new level of complexity to the buffet mechanism (Paladini *et al.* (2019); He & Timme (2021)).

There are two main differences between buffet on airfoils and wings (Hwang & Pi (1975); Riddle (1975); Roos (1985)): 1) on wings, the shock oscillations are non-periodic and feature a broadband spectral signature, and 2), their chordwise excursions are significantly smaller than for airfoil buffet and vary along the wing span (Masini *et al.*, 2019). Iovnovich & Raveh (2015) found that these non-uniformities along the wing span evolve due to occurrence of 3D cellular separation patterns, the buffet cells. These cells are associated with a wave-like shock front propagating in the spanwise direction.

The broadband spectral signature of 3D buffet is associated with Strouhal numbers that are 4 to 7 times higher than for the airfoil scenario (Molton *et al.* (2013); Dandois (2016)): A spanwise analysis of the shock-related frequency spectrum showed a relation between the buffet Strouhal number and the distance between shock and trailing edge, similarly observed for 2D buffet cases (Molton *et al.* (2013); Dandois (2016)).

Iovnovich & Raveh (2015) systematically assessed wing sweep effects by gradually varying sweep angle between 0 and 40 deg on infinite wing configurations. Two principal flow phenomena take place both for swept and unswept wings, although at varying intensity: a distinct λ-shock structure at the inboard wing sections and lateral separation events. For small sweep angles (up to 20 deg), the flow exhibits behavior analogous to the 2D buffet case, characterized by shock wave oscillations predominantly in the chordwise direction. At moderate sweep angles ($20 \leq \Lambda \leq 40$ deg), the classical airfoil buffet vanishes, and lateral pressure communication is enabled. This transition is accompanied by the emergence of spanwise-traveling buffet cells, which are spatially periodic. In addition, both the spanwise propagation speed and the frequency of these buffet cells increase as the sweep angle increases. Iovnovich & Raveh (2015) thus demonstrated a direct correlation between wing sweep and the spectral characteristics of shock-induced unsteadiness.

A modal decomposition of surface pressure data conducted by Masini *et al.* (2019) revealed two characteristic contributions to the frequency spectrum in swept wing buffet: at pre-buffet conditions, a low frequency unsteadiness at $St_c = 0.05 - 0.15$ is propagating in the inboard direction, while a higher frequency ($St_c = 0.2 - 0.5$) broadband contribution was attributed to an outboard propagation confined to the tip region. This observation is consistent with previously reported findings regarding the formation of buffet cells (Iovnovich & Raveh (2015)). With increasing angle of attack, the shock front consistently advances upstream (Masini *et al.*, 2019). Close to buffet onset, and largely independent of the spanwise location, a frequency signature around $St_c = 0.07$, which is characteristic of 2D buffet, was detected. For fully established buffet, higher-frequency components typical of swept wing buffet ($0.2 \leq St_c \leq 0.5$) become important, predominantly concentrated near the wing tip. Overall, these findings support the hypothesis that low-frequency shock unsteadiness centered around 70 Hz persists across the entire span, exhibiting primarily inboard propagation, while higher-frequency oscillations (above 200 Hz) are confined to the outboard wing sections.

Despite many decades research in the field, along with significant advances in both experimental and computational techniques and resources, several questions on the underlying mechanisms and root causes of shock buffet remain unanswered (Nicholas *et al.* (2017)). In view of the numerous applications of supercritical airfoils for aircraft wings and jet engines and a steadily growing demand for efficient and environmentally sustainable air travel, a thorough understanding of the underlying physical mechanism of unsteady periodic transonic flow becomes increasingly relevant. Reliable prediction of buffet onset is not only the prerequisite for the development of measures to effectively control and alleviate the detrimental effects of shock buffet, but also crucial to expand the boundaries of the flight envelope.

However, the vast majority of the (still limited) understanding of transonic buffet has been obtained for the relatively low Reynolds numbers accessible with most laboratory wind tunnels and numerical simulations methods. Reynolds numbers relevant for aircraft flight conditions are about one order of magnitude larger. To contribute to the understanding of buffet in the flight-realistic Reynolds-number regime, we analyze measurements around a full aircraft model in the cryogenic European Transonic Wind Tunnel at a uniquely high Reynolds numbers of $Re = 12.9 \cdot 10^6$ for this study. By discussing the mean and turbulent flow field, we provide insights into the phenomena in the flow regime relevant for aircraft flight conditions. In particular, we analyze a flow configuration in the non-linear flow regime, with an angle of attack of $\alpha = 6.9^\circ$, where the wake of the buffet-prone aircraft wing impinges on the aircraft's tailplane. This case is of particular interest, since studies on 2D tandem-wing configurations have shown that the buffet unsteadiness is affecting the tailplane aerodynamics (Schauerte & Schreyer (2025); Blind *et al.* (2024)).

The article is structured as follows: first, we introduce the experimental setup and approach, followed by a discussion of the overall flow topology and the mean velocity field. Then, we characterize the turbulent velocity field along the wake of the aircraft wing in detail, briefly discussing also potential effects on the tailplane of the aircraft. The article ends with our main conclusions and an outlook.

EXPERIMENTAL SETUP

In this section, we introduce the experimental facility, model, measurement techniques, and data analysis approach.

The European Transonic Wind Tunnel

The European Transonic Windtunnel (ETW) in Cologne, Germany, is a continuously operated cryogenic wind tunnel. The desired high Reynolds numbers are achieved with low temperatures in the test section, for which liquid nitrogen at -196° Celsius is continuously injected into the tunnel flow. The vaporizing liquid nitrogen forms a cold gas flow with total temperatures as low as 110 K and total pressures of up to 450 kPa. The ETW can thus accurately simulate realistic high-lift and high-speed flight conditions of modern passenger aircraft. The test section (height of 2m, width of 2.4m) is encapsulated in an insulated stainless steel pressure shell with a diameter of about 10m. With this pressurized test chamber and an independently adjustable temperature regime, the key parameters (Mach and Reynolds number, and dynamic pressure) can be set and controlled independently.

For the present study, the flow parameters were as follows: Mach number $M = 0.9$; $Re = 12.9 \times 10^6$; total temperature $T_t = 180\ K$; and total pressure $p_t = 230\ kPa$.

Wind-tunnel model

The flow around the full model XRF1 aircraft geometry provided by Airbus was analyzed. The stainless-steel model (total span of 1.56m, mean aerodynamic chord of 0.1965m) was sting-mounted into the ETW test section (see Fig. 1).

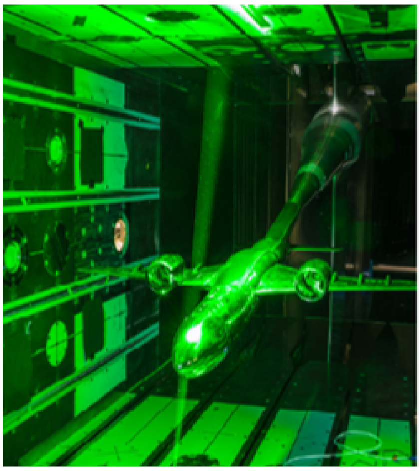

Figure 1. XRF-1 aircraft model installed in the European Transonic Wind Tunnel. Figure from Bosbach *et al.* (2024).

Velocity measurements with particle-image velocimetry (PIV) were carried out along the wake of the aircraft wing. The relative spanwise position of the measurements was set to $\eta = 0.29$, where $\eta = 0$ corresponds to the fuselage centerline and $\eta = 1$ corresponds to the wingtip (see Fig. 2).

Cryogenic particle-image velocimetry setup

The velocity field was measured using the cryoPIV-technique developed by DLR. To analyze both the buffet flow field around the wing and the wake of the wing in detail, measurements were carried out in multiple fields of view (see Fig. 2). Our setup consisted of a) two special multi-pulse "FOX" PIV systems focused on the wing suction side including the trailing edge (plane YZ) and the flow directly upstream of the horizontal tailplane (plane Y) and b) a 3.3 kHz PIV system capturing four fields of view along the wake (planes LA, LB, LC, and LD). All PIV systems are stereoscopic setups, providing access to all three velocity components. Ice crystals were used as PIV seeding particles to prevent damage to the insulation material of the wind tunnel. The measurement system is described in detail in Bosbach *et al.* (2024).

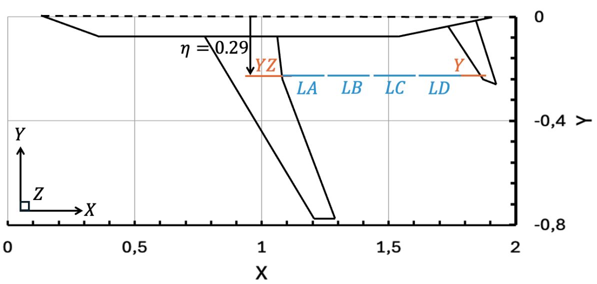

Figure 2. PIV measurement planes. Figure adapted from Bosbach *et al.* (2024).

The use of different camera systems caused slight differences in the measured values, so that the velocity fields in planes Y and YZ look slightly different in Fig. 3 than in the other measurement fields, and the transition of the RMS values is not completely smooth, which is to expect in such challenging conditions. Furthermore, due to the overall complexity of the configuration, the line of sight of the cameras of the measurement field covering the airfoil suction side is directed through the shock region, which leads to increased uncertainty downstream of the shock at $x/c = 0.5$ in this field of view. To improve data quality, a normalized median test was applied to all vectors, removing outliers and increased fluctuations with deviations exceeding 3σ from the local mean. Snapshots with more than 10% outliers are not considered in further analyses.

The stereo velocity fields are based on vector fields calculated at distances between 1.5 × 1.5 to 2 ×2 mm, which corresponds to 1% of the mean aerodynamic chord. The interogation windows are 3 x 3 to 4 x 4 mm.

RESULTS

Global flow topology and mean velocity field

The overall flow topology is visualized in Fig. 3, showing a contour plot of the rms-values of the velocity fluctuations in the wing-surface-normal $z-$direction. Additional contour plots of the other components of the velocity are provided in Bosbach *et al.* (2024). The supersonic region on the suction side terminates with a lambda shock, which induces the separation of the boundary layer on the upper surface of the airfoil. Downstream of the airfoil, the wake is clearly visible. Its intensity reduces quickly downstream of the trailing edge, but the wake is persistent over the entire measurement window ($x/d \geq 4.6$) and also affects the inflow of the tailplane for the present angle of attack. As expected for the asymmetric wing profile, the wake shows asymmetry between the upper and lower surfaces.

Note that the data quality of measurements close to the upper airfoil surface is compromised by the upper wing surface in the background of the images, the limited stereo-angle enforced by the WT window positions and the optical path going through the shock wave. Consequently, the velocity vectors in that measurement region are excluded from the subsequent analysis to ensure reliability of the results.

A quantitative analysis of the mean velocity field is carried out on the basis of mean velocity profiles of the streamwise (see Fig. 4), surface-normal (see Fig. 5), and spanwise (see Fig. 6) velocity components, normalized with the undisturbed flow velocity U_∞ in the x-direction of the model coordinate system. To improve readability, every third data point is highlighted in the Figures.

In the streamwise component, immediately downstream of the trailing edge, at position $x/c = 1.2$, the velocity deficit reaches $u_{mean}/U_\infty = 0.55$, indicating a substantial loss of momentum in the wake of the airfoil. The maximum deficit occurs at $z/c = 0.025$ slightly above the center line. At this streamwise position, the streamwise velocity component is increased by $u_{mean}/U_\infty = 0.04$ below and $u_{mean}/U_\infty = 0.1$ above the center line even upside of the wake core, reflecting the acceleration of the flow around the low velocity wake.

The velocity deficit decreases rapidly with downstream distance and reaches a value of $u_{mean}/U_\infty = 0.85$ at $x/c = 1.5$ in the centerline of the wake. Behind this near-wake region, the wake deficit decreases only slowly, reaching a value of $u_{mean}/U_\infty = 0.95$ at $x/c = 4.0$. Initially, the location of maximum velocity deficit remains almost constant slightly above the centerline; from $x/c = 4.0$ onwards, it moves higher above the centerline. This "upwards bending" of the wake orientation may be due to interactions with the flow around the aircraft fuselage. The fuselage diameter is tapered in the rear section, so that a change in flow direction is expected.

The velocity component in the surface-normal z-direction, w_{mean}/U_∞, shown in Fig. 5, is approximately one

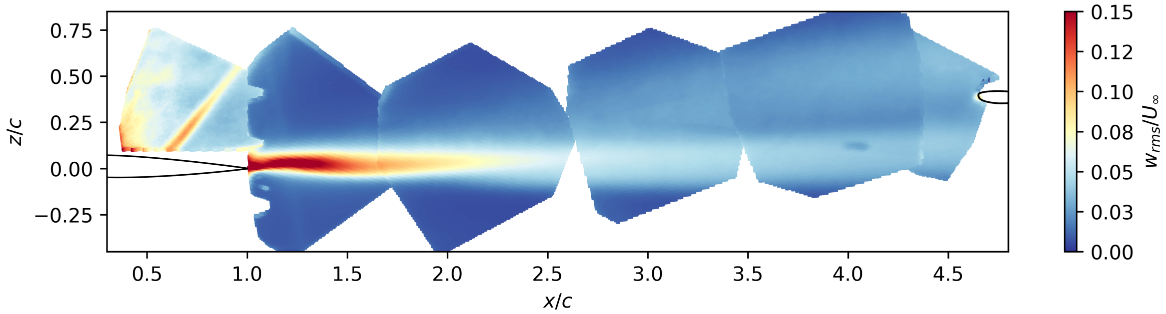

Figure 3. Contour plot of the turbulence component in the surface-normal direction $w_{\mathrm{rms}}/U_\infty$. (NACA airfoil with arbitrary camber and thickness, not the actual airfoil).

order of magnitude smaller than the streamwise component u_{mean}/U_∞. A region of downward-directed velocity ($w_{mean} < 0$) is observed above the airfoil, and below the airfoil, a region of upwards oriented velocity develops ($w_{mean} > 0$). The respective maxima are located immediately downstream of the trailing edge, at the same position as the maximum velocity deficit (see Fig. 4). As the downstream distance increases, the maxima of both regions decrease considerably with the slowly decaying wake. Directly downstream of the wing ($x/c = 1.2$), values of $w_{mean}/U_\infty = -0.15$ and $w_{mean}/U_\infty = 0.1$ are reached above and below the center of the wake, respectively, which change approximately linearly to $w_{mean}/U_\infty = -0.05$ and $w_{mean}/U_\infty = 0.08$, respectively, until $x/c = 4.5$.

The spanwise velocity component exhibits pronounced asymmetry with respect to the wake centerline. Below the airfoil, the velocity component assumes negative values, indicating a spanwise flow, directed towards the wingtip. A maximum in the absolute magnitude of the negative spanwise velocity is observed in the region of strongest wake intensity immediately downstream of the trailing edge at $x/c = 1.2$, with a value of $v_{mean}/U_\infty = -0.2$, at $z/c = 0.1$ above the airfoil chord line. Until $x/c = 2$, this minimum loses much of its intensity $v_{mean}/U_\infty = -0.1$ and shifts downward to $z/c = -0.1$. Further downstream, the minimum remains at this height and continues to loose intensity slowly. The sign change of the spanwise component does not coincide with the geometric centerline but instead occurs at a location above the chord midline, reflecting the asymmetric organization of the wake. With increasing downstream distance, the location of the sign change, moves upwards towards the horizontal tailplane.

The maximum velocity in the spanwise direction occurs at $z/c = 0.2$ (for $x/c = 1.2$), with a value of $v_{mean}/U_\infty = 0.15$. With downstream evolution, this maximum decreases as the velocity decreases and shifts uniformly upward. Beyond $x/c = 4$, the sign change of the spanwise component occurs at significantly elevated positions, specifically above the horizontal stabilizer at $z/c > 0.4$. The pronounced changes in the spanwise velocity component reflect the interaction of the 3D wake flow with the 3D flow around the overall aircraft.

Turbulent velocity field

The turbulent intensities of the velocity components in the main flow direction, u_{rms}/U_∞ (see Fig. 7), the wall-normal direction, w_{rms}/U_∞, (see Fig. 8), and the spanwise direction, v_{rms}/U_∞ (see Fig. 9), all reach their intensity maxima directly downstream of the wing trailing edge. At $x/c = 1.2$, u_{rms}/U_∞ reaches an intensity maximum of 0.22, while w_{rms}/U_∞ and v_{rms}/U_∞ reach slightly lower maxima of 0.18. With increasing downstream distance, the regions of elevated turbulence intensity expand laterally and diminish in intensity for all three components, as expected for a wake flow. The initial decrease downstream of the trailing edge is most rapid. Beyond $x/c = 2$, the diffusion becomes noticeably stronger, and the behaviors of the three components start to deviate. In the u_{rms}/U_∞ component, the intensity maximum remains approximately at the same height and decays by about 86% over the observed downstream distance. The v_{rms}/U_∞ component behaves similarly as the u_{rms}/U_∞ component: both components have a maximum at about $z/c = 0.05$ in the wake core, and decrease in intensity with downstream evolution in the same manner.

In the wall-normal component, the maximum intensity is only reduced by 78% along the wake over the distance observed. The intensity maximum is located at $z/c = 0.05$ only until $x/c \approx 2$; for $x/c > 2$, it shifts significantly upward with downstream evolution, towards $z/c = 0.4$. The w_{rms}/U_∞ component decreases less rapidly, by 50% up until $x/c = 2$, whereas u_{rms}/U_∞ and v_{rms}/U_∞ decrease by 75% and 65%, respectively, over the same distance.

The Reynolds shear-stress profiles are presented in Fig. 10. The very low values of about $\overline{u'w'}/U_\infty^2 = 0.001$ in the free stream away from the wake demonstrate that our CryoPIV system reaches favorably low measurement noise.

In the wake center, the Reynolds stresses $\overline{u'w'}/U_\infty^2$ are equal to 0 at the same vertical location as the maximum speed deficit (see Fig. 6) and the maximum turbulence intensities occur (see Figs. 7, 8, and 9). Above and below this line, there are regions with elevated Reynolds stresses of opposite signs.

The region originating from the suction side of the wing has a higher intensity ($\overline{u'w'}/U_\infty^2 = 0.0185$) than on the pressure side, where $\overline{u'w'}/U_\infty^2 = 0.007$, reflecting the stronger disturbance due to the strongly separated flow. Both intensity peaks decrease at the same rate, which is comparable to the decrease in intensity of the u_{rms} and v_{rms} components. The locations of the intensity extrema remains virtually constant along the observed downstream extent of the wake, namely at $z/c = 0.05$ and $z/c = 0.005$. With downstream evolution, the area with increased Reynolds stresses expands to 1.5 times its original extent, with rapidly decreasing intensity towards its edges. At a distance of $z/c > 0.2$, the Reynolds stress has reduced to free-stream levels above and below the wake core.

Influence on the horizontal tailplane

One objective of the specific case studied here was to create a configuration where the wake of the buffet-dominated flow around the aircraft's wing impinges on the tailplane. Previous studies on 2D configurations have shown that the buffet unsteadiness is imprinted on the tailplane via the wake and affects the tailplane aerodynamics (see Schauerte & Schreyer

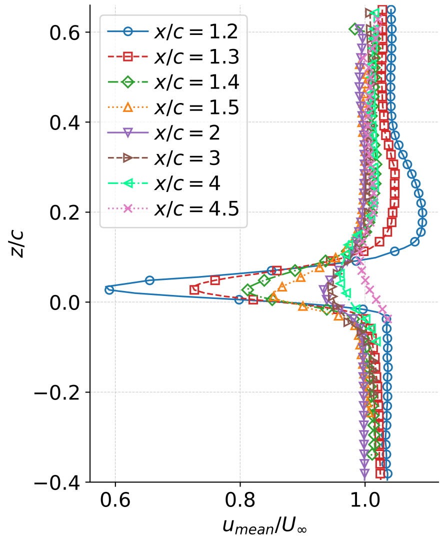

Figure 4. Mean streamwise velocity component

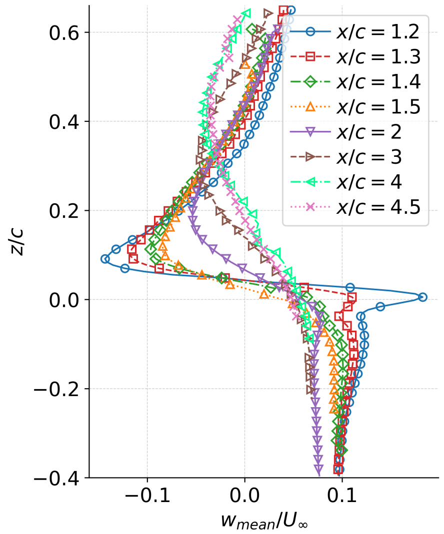

Figure 5. Mean wall-normal velocity component

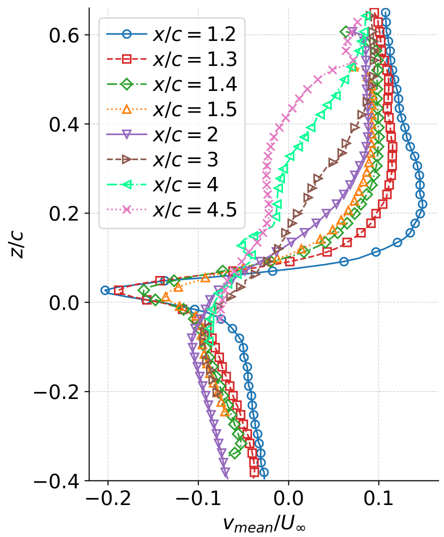

Figure 6. Mean spanwise velocity component

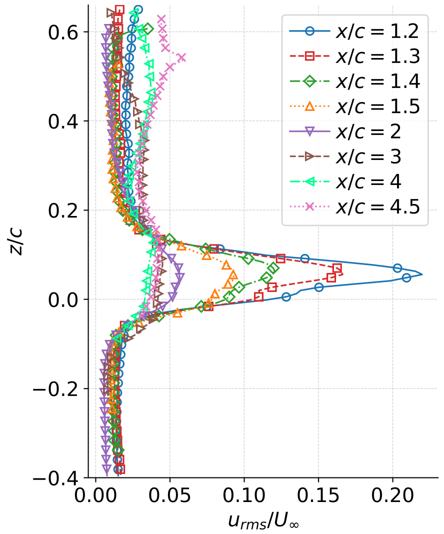

Figure 7. Streamwise turbulence component

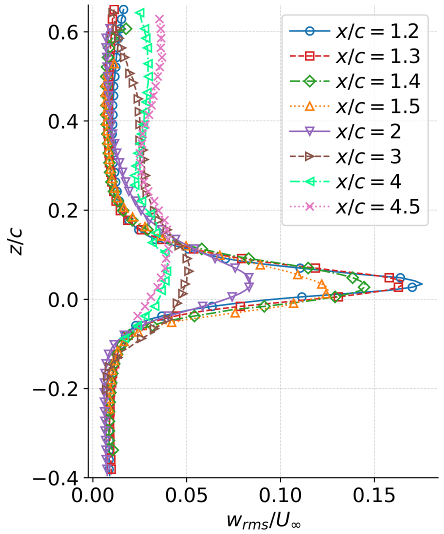

Figure 8. Wall-normal turbulence component

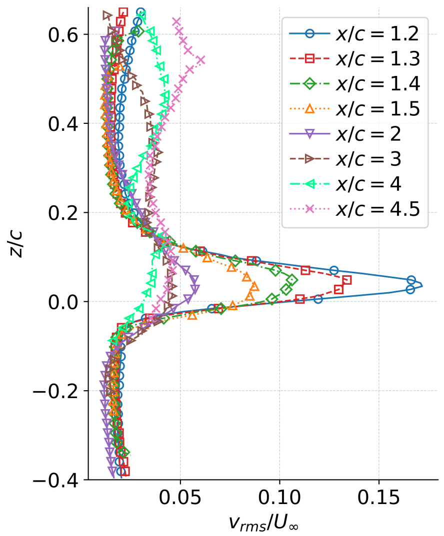

Figure 9. Spanwise turbulence component

(2025); Blind *et al.* (2024)). With the present configuration, the influence of the wake on the tailplane can be studied for a

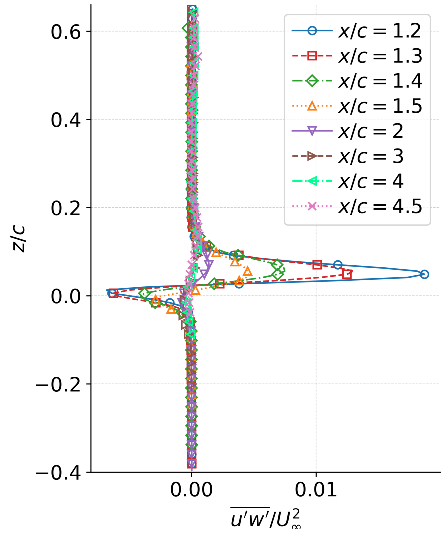

Figure 10. Reynolds shear stress component $\overline{u'w'}/U_\infty^2$

3D configuration and at flight-realistic Reynolds numbers for the first time. The position of the leading edge of the horizontal tailplane is $x/c = 4.66$ and $z/c = 0.4$. In this region, an influence of the wake is clearly visible in the mean surface-normal and spanwise velocity components, both of which have clearly not yet decayed to equilibrium free-stream conditions (see Figs. 5 and 6). The mean streamwise component of the velocity (Fig. 4) seems to not contribute significantly in this region. The turbulent components in all three directions clearly show an interaction with the tail plane. At $x/c = 4.5$, both the streamwise and spanwise components show a distinct intensity peak of around 0.06 centered around $z/c = 0.55$. The surface-normal component only shows a much smoother and weaker intensity increase – a similar trend is also visible at $x/c = 0.4$ for all three turbulence intensity components. The distinct peak discussed above is probably superimposed, and of different origin than the weak increase. In the Reynolds stresses $\overline{u'w'}/U_\infty^2$, a very weak increase in intensity occurs at the same streamwise location and distance from the surface.

CONCLUSIONS AND OUTLOOK

Transonic buffet is one of the most influential unsteady flow phenomena affecting the aerodynamic performance and restricting the flight envelope of modern passenger aircraft. The presented research contributes to our overall objective to advance the understanding of buffet to be able to overcome its detrimental effects. In particular, we present and discuss detailed PIV measurements of transonic wing buffet at flight-realistic Reynolds numbers. Buffet data at such high Reynolds numbers are exceedingly rare, and we provide the first quantitative discussion of the turbulence evolution along the wake of the aircraft wing. We showed also that the present configuration allows us to analyze the interaction between wing wake and horizontal tailplane, where the latter is also affected by the buffet unsteadiness on the wing.

ACKNOWLEDGMENTS

We gratefully acknowledge the German Research Foundation (DFG) for funding this work within the framework of the research unit FOR 2895, subproject TP6 (project 406435057) and the Hightech Agenda Bayern for funding the first author. We would like to thank the Helmholtz Gemeinschaft HGF (Helmholtz Association), Deutsches Zentrum für Luft- und Raumfahrt DLR (German Aerospace Center), and Airbus for providing the wind tunnel model and financing the wind tunnel measurements, as well as public support to mature the test methods applied by DLR and ETW.

REFERENCES

Benoit, B. & Legrain, I. 1987 Buffeting prediction for transport aircraft applications based on unsteady pressure measurements. *AIAA 5th Applied Aerodynamics Conference* .

Blind, M. P., Gibis, T., Wenzel, C. & Beck, A. 2024 Wall-modeled large eddy simulation of a tandem wing configuration in transonic flow. *Physics of Fluids* **63**, 055125.

Bosbach, J., Konrath, R., Geisler, R., Philipp, F., Agocs, J., Kühn, C. & Koop, L. 2024 Capturing unsteady flow phenomena at high speed stall conditions by adaptation and application of cryogenic piv. In *AIAA SCITECH 2024 Forum*, pp. 1–19. Orlando, FL: American Institute of Aeronautics and Astronautics.

Crouch, J. D., Garbaruk, A., Magidov, D. & Travin, A. 2009 Origin of transonic buffet on aerofoils. *Journal of Fluid Mechanics* **628**, 357–369.

Dandois, J. 2016 Experimental study of transonic buffet phenomenon on a 3d swept wing. *Physics of Fluids* **28** (1), 016101.

Eckstrom, C. V., Seidel, D. A. & Sandford, M. C. 1990 Unsteady pressure and structural response measurements on an elasticsupercritical wing. *Journal of Aircraft* **27** (1), 75–80.

He, W. & Timme, S. 2021 Triglobal infinite-wing shock-buffet study. *Journal of Fluid Mechanics* **925**, A27.

Hwang, C. & Pi, W.S. 1975 Northrop f-5a aircraft transonic buffet pressure data acquisition and response analysis. *Journal of Aircraft* **12** (9), 714–720.

Iovnovich, M. & Raveh, D. E. 2015 Numerical study of shock buffet on three-dimensional wings. *AIAA Journal* **53** (2), 449–463.

Kenway, G. KW & Martins, J. RRA 2017 Buffet-onset constraint formulation for aerodynamic shape optimization. *AIAA Journal* **55** (6), 1930–1947.

Masini, L., Timme, S. & Peace, A. J. 2019 Analysis of a civil aircraft wing transonic shock buffet experiment. *Journal of Fluid Mechanics* **884**.

Molton, P., Dandois, J., Lepage, A., Brunet, V. & Bur, R. 2013 Control of buffet phenomenon on a transonic swept wing. *AIAA Journal* **51** (4), 761–772.

Nicholas, F. G., Gareth, A. V. & Oleg, L. 2017 A review of recent developments in the understanding of transonic shock buffet. *Progress in Aerospace Sciences* **92**, 39–84.

Paladini, E., Dandois, J., Sipp, D. & Robinet, J.-Ch. 2019 Analysis and comparison of transonic buffet phenomenon over several three-dimensional wings. *AIAA Journal* **57** (1), 379–396.

Riddle, D. 1975 Wind-tunnel investigation of surface-pressure fluctuations associated with aircraft buffet. In *13th Aerospace Sciences Meeting*, p. 67.

Roos, F. 1985 The buffeting pressure field of a high-aspect-ratio swept wing. In *18th Fluid Dynamics and Plasmadynamics and Lasers Conference*, p. 1609.

Schauerte, C. J. & Schreyer, A.-M. 2025 On the wake/tailplane interaction for established transonic airfoil buffet. *AIAA Journal* **63** (7), 2731–2749.

Stanewsky, E. & Basler, D. B. 1990 Experimental investigation of buffet onset and penetration on a supercritical airfoil at transonic speeds. *AGARD Conference Proceedings* **483**.